



Cite this: *CrystEngComm*, 2025, 27, 4404

Zn(II), Cd(II) and Hg(II) halide coordination polymers supported by bis-pyridyl-bis-amide: structural diversity and structural transformation†

Arigna Rasphone, Hong-Chuan Zhang, Yun-Syuan Lee, Yu-Hui Ye, Ying-Tong Kuo, Yi-Fang Lai, Zhi-Ling Chen, Song-Wei Wang and Jhy-Der Chen  *

Reactions of metal halide with *N,N'*-bis(3-pyridylmethyl)oxalamide (L^1), *N,N'*-bis(4-methylpyridyl)oxalamide (L^2) or *N,N'*-bis(3-methylpyridyl)adipamide (L^3) afforded $\{[ZnI_2(L^1)]\cdot2DMF\}_n$, **1**, $[ZnI_2(L^1)]_n$, **2**, $[CdI_2(L^1)]_n$, **3**, $[HgI_2(L^1)]_n$, **4**, $[HgI_2(L^2)]_n$, **5**, $[Hg_2I_4(L^3)]_n$, **6**, $[CdI_2(L^3)]_n$, **7**, 1D-[$CdBr_2(L^1)_2$]_{*n*}, **8**, 2D-[$CdBr_2(L^1)_2$]_{*n*}, **9**, and $[Cd_2Br_2(ox)(L^1)_2]_n$ (ox^- = oxalate), **10**, whereas the reaction of $Cd(CH_3COO)_2\cdot2H_2O$ with L^1 gave $\{[Cd(ox)(L^1)]\cdot4H_2O\}_n$, **11**, which have been structurally characterized by using single-crystal X-ray diffraction. Complexes **1** and **2** form a pair of supramolecular isomers, giving a 1D concavo-convex chain and a 1D zigzag chain, respectively, whereas **3**, **4**, **5** and **7** are 1D zigzag chains and **6** is a dinuclear complex, demonstrating that the solvent identity and the length of the spacer ligand are important in determining the structural diversity. Complexes **8** and **9** are another pair of supramolecular isomers, adopting a 1D looped-chain and a 2D layer with the (4⁴.6²)-sql topology, respectively. Complex **10** is a 3D framework with the (6⁶)-dia topology and **11** is a 2D layer with the (4⁴.6²)-sql topology. Moreover, complexes **1** and **2** display irreversible structural transformation upon solvent removal, whereas temperature-dependent structural transformations from **8** to **9**, **8** to **10** and **9** to **10** are observed.

Received 4th May 2025,

Accepted 21st May 2025

DOI: 10.1039/d5ce00465a

rsc.li/crystengcomm

Introduction

The rational design and synthesis of coordination polymers (CPs) have been rapidly developing, due to their fascinating structural diversity and potential applications in magnetism, gas storage and separation, drug delivery, catalysis, luminescence, sensing, and so on.^{1–8} The properties of CPs are mostly dominated by their structures and compositions and it is well known that the structural type of CPs is affected by many factors, including metal ions, counterions, temperature and identity of the organic linker. Metal-to-ligand ratios and solvent systems are also significant in the preparation of CPs.^{9–12} Therefore, controlling the appropriate factors to construct suitable CPs has become an exciting topic in the crystal engineering of CPs. On the other hand, structural transformations of CPs that lead to the formation of intriguing structures have attracted great attention of the researchers.^{13–21}

One-dimensional (1D) CPs based on Zn(II), Cd(II) and Hg(II) halide have been reported, however, it remains a

challenge to elucidate their structure–ligand relationship and thereby the intrinsic properties.^{22–30} We have investigated the structural diversity and properties of the CPs constructed from the bis-pyridyl-bis-amide ligand (bpba) and Hg(II) that exhibited structural transformations. Reversible structural transformation between $[Hg(1,3-pbpa)X_2]_n$ [X = Br and I; 1,3-pbpa = 2,2'-(1,3-phenylene)-bis(*N*-(pyridin-3-yl)acetamide)] and $[Hg(1,3-pbpa)X_2\cdot MeCN]_n$ was ascribed to the formation and breaking of the N–H···N hydrogen bonds to the acetonitrile molecules.²³ On the other hand, 1D mercury(II) chloride CPs synthesized by using a semi-rigid N-donor ligand, 2,2'-(1,4-phenylene)-bis(*N*-(pyridin-3-yl)acetamide) (1,4-pbpa), $[Hg(1,4-pbpa)Cl_2\cdot CH_3OH]_n$ and $[Hg(1,4-pbpa)Cl_2]_n$ underwent reversible structural transformation upon removal and uptake of CH_3OH . Pyridyl ring rotation of the 1,4-pbpa ligand that results in the change of the ligand conformation was proposed for the initiation of the structural transformation.²⁴

To investigate the effect of metal identity and ligand flexibility on the structural diversity of the metal halide CPs and to elucidate the factors that may govern the structural transformations, ten new CPs and a dinuclear complex containing bpba, *N,N'*-bis(3-pyridylmethyl)oxalamide (L^1), *N,N'*-bis(4-methylpyridyl)oxalamide (L^2) or *N,N'*-bis(3-methylpyridyl) adipamide (L^3), namely $\{[ZnI_2(L^1)]\cdot2DMF\}_n$, **1**, $[ZnI_2(L^1)]_n$, **2**, $[CdI_2(L^1)]_n$, **3**, $[HgI_2(L^1)]_n$, **4**, $[HgI_2(L^2)]_n$, **5**, $[Hg_2I_4(L^3)]_n$, **6**,

Department of Chemistry, Chung Yuan Christian University, Chung-Li, Taiwan, Republic of China. E-mail: jdchen@cycu.edu.tw

† Electronic supplementary information (ESI) available: Packing diagrams (Fig. S1–S3). PXRD patterns (Fig. S4–S14). CCDC no. 2445340–2445350 contain the supplementary crystallographic data for this paper. For ESI and crystallographic data in CIF or other electronic format see DOI: <https://doi.org/10.1039/d5ce00465a>



$[\text{CdI}_2(\text{L}^3)]_n$, **7**, 1D- $[\text{CdBr}_2(\text{L}^1)]_n$, **8**, 2D- $[\text{CdBr}_2(\text{L}^1)]_n$, **9**, $[\text{Cd}_2\text{Br}_2(\text{ox})(\text{L}^1)]_n$ (ox = oxalate), **10**, and $\{[\text{Cd}(\text{ox})(\text{L}^1)]\cdot 4\text{H}_2\text{O}\}_n$, **11**, are prepared. Fig. 1 depicts the structures of L^1 , L^2 and L^3 . The synthesis and structural characterization of these complexes form the subject of this report. Irreversible structural transformation from complex **1** to complex **2** upon DMF removal and the temperature-dependent structural transformations in **8–10** are also discussed.

Experimental details

General procedures

IR spectra (KBr disk) were obtained from a JASCO FT/IR-4200 FT-IR spectrometer. Elemental analyses were performed on an Elementar vario EL III analyzer. Powder X-ray diffraction was carried out on a Bruker D2 PHASER diffractometer with $\text{CuK}\alpha$ ($\lambda_{\alpha} = 1.54 \text{ \AA}$) radiation.

Materials

The reagent zinc iodide was purchased from Nova, cadmium iodide from Alfa Aesar, mercury iodide from Sigma-Aldrich and cadmium bromide from Strem Chemicals, Inc. The ligands *N,N'*-bis(3-pyridylmethyl)oxalamide (L^1), *N,N'*-bis(4-methylpyridyl)oxalamide (L^2) and *N,N'*-bis(3-methylpyridyl) adipamide (L^3) were prepared according to published procedures.³¹

Preparation of $\{[\text{ZnI}_2(\text{L}^1)]\cdot 2\text{DMF}\}_n$, 1. L^1 (0.24 g, 1.0 mmol) was placed in a flask containing 15 mL of DMF, and ZnI_2 (0.32 g, 1.0 mmol) was added. The mixture was then heated at reflux for 24 h to afford a yellow solution with some white solids. Colorless crystals suitable for single crystal X-ray diffraction were obtained by slow diffusion of diethyl ether into the DMF solution for several weeks. Yield: 0.36 g (49%). Anal. calcd for $\text{C}_{20}\text{H}_{28}\text{ZnI}_2\text{N}_6\text{O}_4$ (MW = 735.65 g mol⁻¹): C, 32.62; N, 11.42; H, 3.81%. Found: C, 28.78; N, 9.78; H, 2.40%.

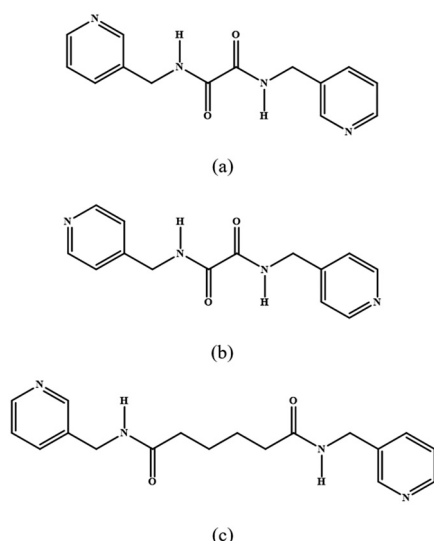


Fig. 1 Structures of (a) L^1 , (b) L^2 and (c) L^3 .

Anal. calcd for $\text{C}_{20}\text{H}_{28}\text{ZnI}_2\text{N}_6\text{O}_4$ – 2 DMF (MW = 589.48): C, 28.49; N, 9.49; H, 2.37%.

Preparation of $[\text{ZnI}_2(\text{L}^1)]_n$, 2. Complex **2** was prepared by following the same procedures as **1**. When the crystals were exposed to air, the DMF solvents evaporated to give **2** and several crystals were suitable for X-ray crystallography. Yield: 0.36 g (61%). Anal. calcd for $\text{C}_{14}\text{H}_{14}\text{ZnI}_2\text{N}_4\text{O}_2$ (MW = 589.48 g mol⁻¹): C, 28.49; N, 9.49; H, 2.37%. Found: C, 28.90; N, 9.82; H, 2.43%. FT-IR (cm⁻¹): 3318(s), 3048(s), 2931(s), 1663(s), 1515(s), 1438(s), 1212(w), 1111(w), 1050(s), 971(s), 831(w), 672(w), 511(s).

Preparation of $[\text{CdI}_2(\text{L}^1)]_n$, 3. A mixture of CdI_2 (0.037 g, 0.10 mmol) and L^1 (0.027 g, 0.10 mmol) in 1.25 mL of EtOH and 1.25 mL of H_2O was sealed in a 23 mL Teflon-lined steel autoclave, which was heated under autogenous pressure to 120 °C for two days, and then cooled down to room temperature for two days. Colorless crystals were obtained. Yield: 0.059 g (93%). Anal. calcd for $\text{C}_{14}\text{H}_{14}\text{CdI}_2\text{N}_4\text{O}_2$ (MW = 636.49 g mol⁻¹): C, 26.39; N, 8.79; H, 2.20%. Found: C, 25.89; N, 8.85; H, 2.18%. FT-IR (cm⁻¹): 3316(s), 3046(m), 2929(s), 1862(m), 1660(s), 1512(s), 1432(s), 1350(w), 1209(w), 1104(w), 1040(s), 965(s), 825(w), 698(s), 618(w), 506(s).

Preparation of $[\text{HgI}_2(\text{L}^1)]_n$, 4. Complex **4** was prepared by following the same procedures as **3**, except that a mixture of HgI_2 (0.045 g, 0.1 mmol) and L^1 (0.027 g, 0.1 mmol) was used. Colorless crystals were obtained. Yield: 0.066 g (91%). Anal. calcd for $\text{C}_{14}\text{H}_{14}\text{HgI}_2\text{N}_4\text{O}_2$ (MW = 724.68 g mol⁻¹): C, 23.18; N, 7.70; H, 1.93%. Found: C, 23.04; N, 8.20; H, 1.67%. FT-IR (cm⁻¹): 3318(s), 3045(s), 2929(s), 1922(m), 1616(w), 1460(w), 1352(w), 1212(w), 1194(m), 1070(w), 804(m), 700(s), 622(w), 509(s).

Preparation of $[\text{HgI}_2(\text{L}^2)]_n$, 5. Complex **5** was prepared by following the same procedures as **3**, except that a mixture of HgI_2 (0.045 g, 0.10 mmol) and L^2 (0.027 g, 0.10 mmol) in 10 mL EtOH was used. Colorless crystals were obtained. Yield: 0.028 g (39%). Anal. calcd for $\text{C}_{14}\text{H}_{14}\text{HgI}_2\text{N}_4\text{O}_2$ (MW = 724.68 g mol⁻¹): C, 23.20; H, 1.95; N, 7.73%. Found: C, 23.00; H, 1.70; N, 8.03%. FT-IR (cm⁻¹): 3430(s), 2817(w), 2727(w), 2375(w), 2343(w), 1597(s), 1385(m), 1352(m), 1124(w), 768(w), 617(m).

Preparation of $[\text{Hg}_2\text{I}_4(\text{L}^3)]_n$, 6. Complex **6** was prepared by following the same procedures as **3**, except that a mixture HgI_2 (0.045 g, 0.10 mmol) and L^3 (0.033 g, 0.10 mmol) in 1.25 mL H_2O and 1.25 mL EtOH was used. Colorless crystals were obtained. Yield: 0.018 g (29%). Anal. calcd for $\text{C}_{18}\text{H}_{22}\text{Hg}_2\text{I}_4\text{N}_4\text{O}_2$ (MW = 1235.17): C, 17.50; N, 4.54; H, 1.80%. Found: C, 17.49; N, 4.99; H, 1.55%. FT-IR (cm⁻¹): 3440(s), 3240(s), 3073(m), 2926(w), 2857(w), 2820(w), 2370(w), 2344(w), 1647(s), 1599(s), 1478(w), 1439(w), 1386(m), 1351(m), 1268(w), 1191(w), 1134(w), 1048(w), 698(w).

Preparation of $[\text{CdI}_2(\text{L}^3)]_n$, 7. Complex **7** was prepared by following the same procedures as **3**, except that a mixture of CdI_2 (0.037 g, 0.10 mmol) and L^3 (0.033 g, 0.10 mmol) was used. Colorless crystals were obtained. Yield: 0.026 g (38%). Anal. calcd for $\text{C}_{18}\text{H}_{22}\text{CdI}_2\text{N}_4\text{O}_2$ (MW = 692.61): C, 31.21; N, 8.09; H, 3.20%. Found: C, 31.54; N, 8.43; H, 2.91%. FT-IR (cm⁻¹): 3440(s), 2820(w), 2370(w), 2340(w), 1600(s), 1380(m), 1350(m), 768(m), 610(m), 521(m).

Preparation of 1D-[CdBr₂(L¹)₂]_n, 8. A mixture of CdBr₂ (0.054 g, 0.20 mmol) and L¹ (0.027 g, 0.10 mmol) were placed in a 23 mL Teflon reaction flask containing 10 mL H₂O, which was sealed and heated at 100 °C for 48 hours under autogenous pressure and then the reaction system was cooled to room temperature at a rate of 2 °C per hour. Transparent crystals suitable for single-crystal X-ray diffraction were obtained. Yield: 0.013 g (8%). Anal. calcd for C₂₈H₂₈Br₂CdN₈O₄ (MW = 812.79): C, 41.37; H, 3.47; N, 13.79%. Found: C, 41.15; H, 3.18; N, 13.84%. FT-IR (cm⁻¹): 3303(s), 3198(w), 3051(w), 2921(w), 1661(s), 1573(w), 1510(s), 1426(w), 1326(w), 1187(m), 1048(m), 918(w), 758(m), 704(s), 633(m), 523(w).

2D-[CdBr₂(L¹)₂]_n, 9. Complex 9 was prepared by following the same procedures as 8, except that the mixture was heated at 120 °C for 48 hours. Suitable white crystals were obtained. Yield: 0.018 g (11%). Anal. calcd for C₂₈H₂₈Br₂CdN₈O₄ (MW = 812.79): C, 41.37; H, 3.47; N, 13.79%. Found: C, 41.27; H, 3.19; N, 13.87%. FT-IR (cm⁻¹): 3374(s), 3261(s), 3059(w), 2942(w), 1665(s), 1586(s), 1494(s), 1426(m), 1372(w), 1208(w), 1036(w), 935(w), 771(m), 700(s), 611(m), 536(w).

[Cd₂Br₂(ox)(L¹)₂]_n, 10. Complex 10 was prepared by following the same procedures as 8, except that the mixture was heated at 140 °C for 48 hours. Transparent crystals were obtained. Yield: 0.012 g (12%). Anal. calcd for C₃₀H₂₈Br₂Cd₂N₈O₈ (MW = 1013.22): C, 35.56; H, 2.78; N, 11.06%. Found: C, 35.74; H, 2.67; N, 11.41%. FT-IR (cm⁻¹): 3354(s), 3269(w), 3043(w), 2938(w), 1674(s), 1620(s), 1502(s), 1435(w), 1300(w), 1174(m), 1023(w), 947(w), 788(m), 704(s), 620(m), 502(w).

{[Cd(ox)(L¹)₂]_n·4H₂O}, 11. A mixture of Cd(CH₃COO)₂·2H₂O (0.027 g, 0.10 mmol) and L¹ (0.027 g, 0.10 mmol) in 5 mL of H₂O was sealed in a 23 mL Teflon-lined steel autoclave, which was heated under autogenous pressure to 120 °C for two days, and then cooled down to room temperature for two days. Colorless crystals were obtained. Yield: 0.0062 g (11%). Anal. calcd for C₁₆H₂₂CdN₄O₁₀ (MW = 542.78): C, 35.41; N, 10.32; H, 4.09%. Found: C, 35.51; N, 10.59; H, 3.85%. FT-IR (cm⁻¹): 3286(s), 3049(m), 1652(s), 1520(s), 1432(s), 1306(m), 1191(m), 1106(w), 1035(w), 947(w), 793(m), 708(m), 647(m), 496(w), 409(w).

X-ray crystallography

The diffraction data for complexes 1–11 were collected on a Bruker AXS SMART APEX II CCD diffractometer, which was equipped with a graphite-monochromated Mo K_α (λ_{α} = 0.71073 Å) radiation. Data reduction was carried out by standard methods with the use of well-established computational procedures.³² The structure factors were obtained after Lorentz and polarization corrections. An empirical absorption correction based on “multi-scan” was applied to the data. The position of some of the heavier atoms were located by the direct or Patterson method. The remaining atoms were found in a series of alternating difference Fourier maps and least-squares refinements, while the hydrogen atoms except those of the water molecules were added by using the HADD command in

SHELXTL 6.1012.³³ Table S1† lists the crystal data for 1–11. The alerts A and B appealing in the checkcif of complex 2 are presumably due to the poor crystallinity of the crystal used for the measurement. The crystals of complex 2 were obtained fortunately by exposing the crystals of 1 to air, as shown in the Experimental section.

Results and discussion

Structure of {[ZnI₂(L¹)₂]·2DMF}_n, 1

Single-crystal X-ray diffraction analysis shows that complex 1 crystallizes in the monoclinic space group *P*2₁/*n* and each asymmetric unit consists of one Zn(II) cation, one L¹ ligand, two iodide anions and two coordinated DMF molecules. The Zn(II) metal center is four-coordinated by two pyridyl nitrogen atoms from two L¹ ligands [Zn–N = 2.056(3)–2.058(3) Å] and two iodine atoms [Zn–I = 2.5466(6)–2.5579(6) Å], forming a distorted tetrahedral geometry (Fig. 2(a)). The Zn(II) ions are linked together by L ligands to afford a 1D concavo-convex chain (Fig. 2(b) top). Looking down the 1D chain, it is seen that the ZnI₂ groups are located on the right and left sides alternately (Fig. 2(b) bottom). Moreover, the 1D concavo-convex chain is reinforced by the N–H···O hydrogen bonds from the amine hydrogen atoms of L¹ to the oxygen atoms of the adjacent L¹ (H···O = 2.423 Å; \angle N–H···O = 136.1°) and DMF (H···O = 2.090 Å; \angle N–H···O = 144.1°) (Fig. 2(c)).

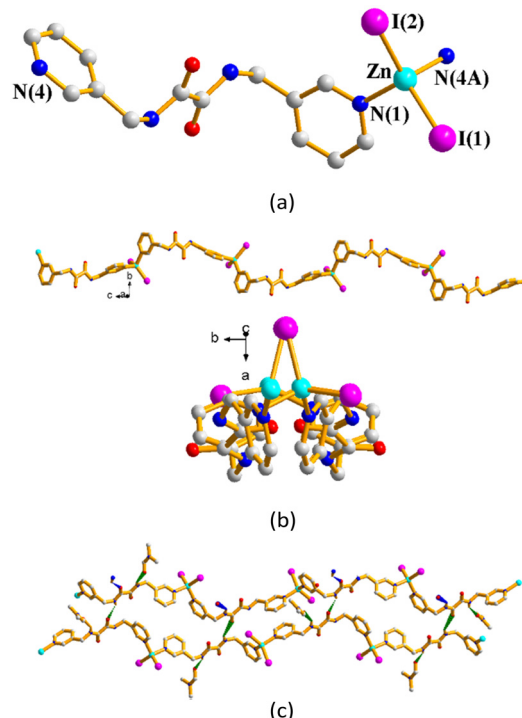


Fig. 2 (a) Coordination environment of the Zn(II) ion in 1. Symmetry transformations used to generate equivalent atoms: (A) $1/2 + x$, $3/2 + y$, $1/2 + z$. (b) a drawing showing the 1D chain of 1, top, and a view looking down the chain, bottom. (c) A drawing showing the N–H···O hydrogen bonds.



Structures of $[M\text{I}_2(\text{L}^1)]_n$ ($M = \text{Zn}$, 2; Cd , 3; Hg , 4)

Crystals of complexes 2, 3 and 4 are isomorphous, which conform to the monoclinic space group $P\bar{1}$ with the asymmetric unit consisting of one $M(\text{II})$ cation, one L^1 ligand, and two iodide anions. The $M(\text{II})$ metal center is four-coordinated by two different pyridyl nitrogen atoms from two different L^1 ligands [$M\text{-N} = 1.991(15)$ and $2.004(13)$ Å for 2; $2.290(5)$ and $2.330(5)$ Å for 3; $2.396(7)$ and $2.464(8)$ Å for 4] and two iodine atoms [$M\text{-I} = 2.476(5)$ and $2.484(5)$ Å for 2; $2.6869(6)$ and $2.6952(6)$ for 3; $2.6418(8)$ and $2.6533(8)$ for 4], forming a distorted tetrahedral geometry (Fig. 3(a)). It is noted that while the $M\text{-N}$ distances increase with the increasing of the size, $\text{Zn}(\text{II}) < \text{Cd}(\text{II}) < \text{Hg}(\text{II})$, the $\text{Cd}\text{-I}$ distances are significantly longer than those of $\text{Zn}\text{-I}$ and $\text{Hg}\text{-I}$.

The $M(\text{II})$ ions are linked together by L^1 ligands to afford 1D zigzag chains (Fig. 3(b), top). Looking down the 1D chain, it is shown that the $M\text{I}_2$ groups are located in an eclipsed fashion (Fig. 3(b) bottom), which are attributed to the ZnI_2 groups in complex 1. Moreover, the 1D zigzag chains are linked by pairs of complementary $\text{N-H}\cdots\text{O}$ hydrogen bonds

from the amine hydrogen atoms of L^1 to the oxygen atoms of the adjacent L^1 ($\text{H}\cdots\text{O} = 2.073$, 2.458 Å and $\angle\text{N-H}\cdots\text{O} = 131.7$, 107.1° for 2; $\text{H}\cdots\text{O} = 2.236$, 2.523 Å and $\angle\text{N-H}\cdots\text{O} = 127.4$, 114.6° for 3; $\text{H}\cdots\text{O} = 2.223$, 2.592 Å and $\angle\text{N-H}\cdots\text{O} = 129.3$, 109.7° for 4) (Fig. 3(c)).

Structure of $[\text{HgI}_2(\text{L}^2)]_n$, 5

Complex 5 crystallizes in the monoclinic space group $P2/n$ and each asymmetric unit consists of a half of a $\text{Hg}(\text{II})$ cation, a half of an L^2 ligand and one iodide anion. Fig. 4(a) depicts the coordination environment of the $\text{Hg}(\text{II})$ ion, which is coordinated by two pyridyl nitrogen atoms from two L^2 ligands [$\text{Hg-N} = 2.466(6)$ Å] and two iodine anions [$\text{Hg-I} = 2.6510(6)$ Å], resulting in a distorted tetrahedral geometry. The HgI_2 units are linked by the L^2 ligands to form a 1D zigzag chain (Fig. 4(b)). The dinuclear molecules are linked through the extensive self-complementary $\text{N-H}\cdots\text{O}$ ($\text{H}\cdots\text{O} = 2.173(4)$ Å; $\angle\text{N-H}\cdots\text{O} = 151.7(4)$) to form a 2D layer (Fig. 4(c)). No $\text{Hg}\cdots\text{I}$ interaction can be observed in this complex.

Structure of $[\text{Hg}_2\text{I}_4(\text{L}^3)]_n$, 6

Complex 6 crystallizes in the monoclinic space group $C2/c$ and each asymmetric unit consists of one $\text{Hg}(\text{II})$ cation, a half

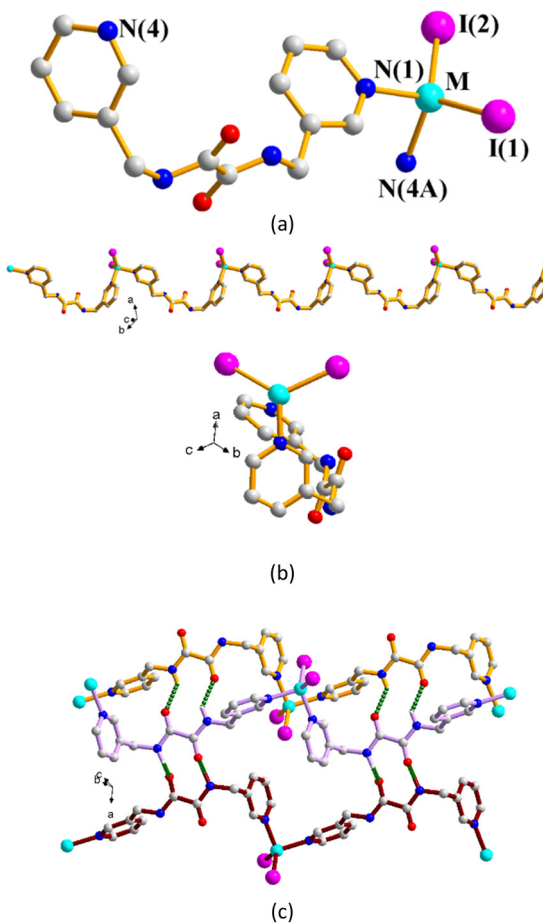


Fig. 3 (a) A representative drawing showing the coordination environment of the $M(\text{II})$ ion in 2–4. Symmetry transformations used to generate equivalent atoms: (A) $1 + x$, $1 + y$, $1 + z$. (b) A drawing showing the 1D chain of 2–4. (c) A drawing showing the $\text{N-H}\cdots\text{O}$ hydrogen bonds.

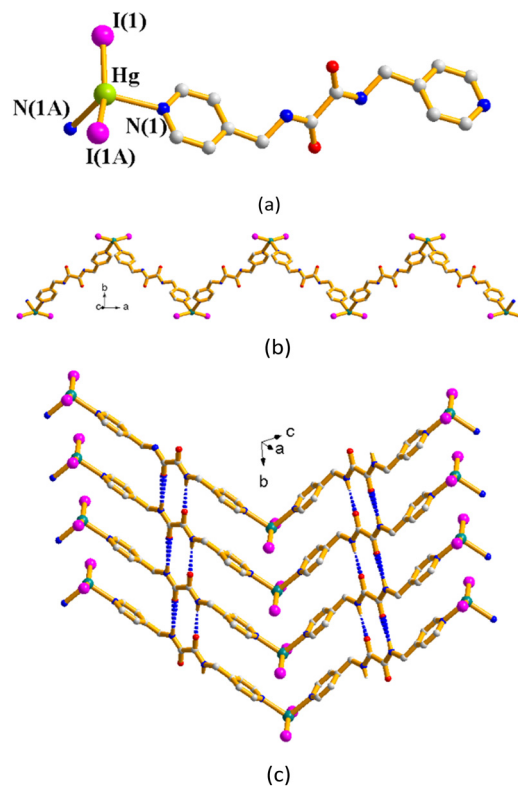


Fig. 4 (a) Coordination environment of the $\text{Hg}(\text{II})$ ion in 5. Symmetry transformations used to generate equivalent atoms: (A) $-x + 1/2$, y , $-z + 1/2$. (b) A drawing showing the 1D chain. (c) A drawing showing the 2D layer supported by the self-complementary $\text{N-H}\cdots\text{O}$ hydrogen bonds.



of an L^3 ligand and two iodide anions. Complex **6** forms a dinuclear structure and each of the two $Hg^{(II)}$ metal centers is three-coordinated by one pyridyl nitrogen atom from the L^3 ligand [$Hg-N = 2.370(5)$ Å] and two iodine atoms [$Hg-I = 2.6198(5)$ and $2.6481(4)$ Å], forming a distorted triangular planar geometry (Fig. 5(a)). The dinuclear molecules are linked through the $Hg\cdots I$ [3.4540(7) Å] interactions and self-complementary $N-H\cdots O$ ($H\cdots O = 1.828(7)$ Å; $\angle N-H\cdots O = 169.4(5)$) to form a 1D band (Fig. 5(b)).

Structure of $[CdI_2(L^3)]_n$, **7**

Complex **7** crystallizes in the monoclinic space group *Cc* and each asymmetric unit consists of one $Cd^{(II)}$ cation, one L^3 ligand and two iodide anions. Fig. 6(a) depicts a drawing showing the coordination environment of the $Cd^{(II)}$ ion of **7**, which is four-coordinated by two pyridyl nitrogen atoms from two L^3 ligands [$Cd-N = 2.248(8)$ and $2.280(8)$ Å] and two iodine atoms [$Cd-I = 2.6783(13)$ and $2.7095(13)$ Å], forming a distorted tetrahedral geometry. The $Cd^{(II)}$ ions are linked by the L^3 ligands to form a concavo-convex chain (Fig. 6(b)). The 1D chains are linked through $N-H\cdots O$ ($H\cdots O = 1.985(9)$ and $2.200(12)$ Å; $\angle N-H\cdots O = 170.9(6)$ and $132.4(8)^\circ$) hydrogen bonds (Fig. 6(c)) to form a 2D layer.

Structure of 1D- $[CdBr_2(L^1)_2]_n$, **8**

The single-crystal X-ray diffraction analysis shows that **8** crystallizes in the monoclinic space group *Pi*. The symmetric unit consists of one $Cd^{(II)}$ cation and two L^1 ligands. Fig. 7(a) shows the coordination environment of the $Cd^{(II)}$ metal center, which is six-coordinated by its two original bromine

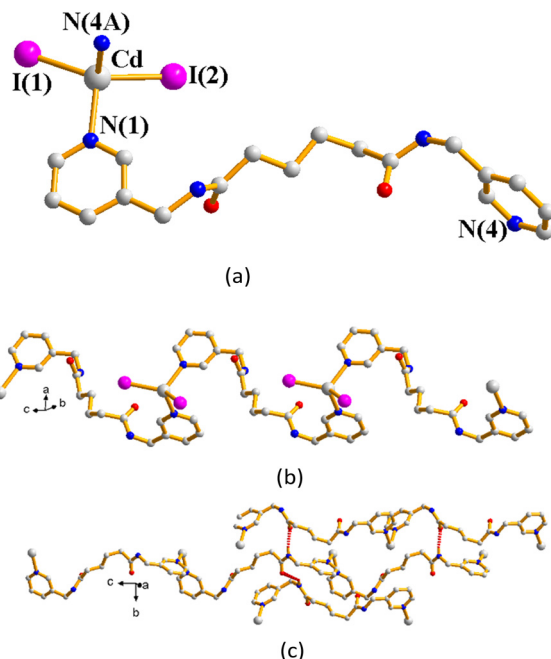


Fig. 6 (a) A drawing showing the coordination environment of the $Cd^{(II)}$ ion of **7**. Symmetry transformations used to generate equivalent atoms: (A) $-x, -y + 2, -z$. (b) A drawing showing the 1D zigzag chain. (c) The 1D chains are linked through $N-H\cdots O$ hydrogen bonds.

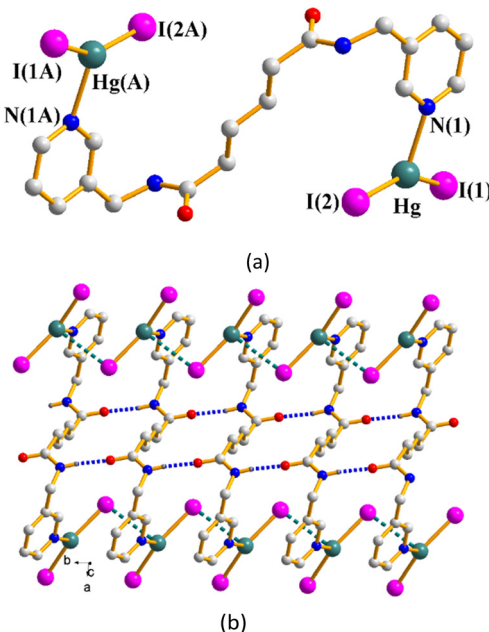


Fig. 5 (a) A drawing showing the dinuclear structure of **6**. Symmetry transformations used to generate equivalent atoms: (A) $-x, -y + 2, -z$. (b) The dinuclear molecules are linked through $Hg\cdots I$ interactions and $N-H\cdots O$ hydrogen bonds.

atoms [$Cd-Br = 2.6937(13)$ Å] and four nitrogen atoms from four different ligands [$Cd-N = 2.3910(3)$ and $2.5020(3)$ Å]. The $Cd^{(II)}$ central metal atom is bridged by two different L^1 , both horizontally to form a 1D looped-chain (Fig. 7(b)). If the $Cd^{(II)}$ ions are considered as four-connected nodes and the L^1 ligands as two-connected nodes, the structure of **8** can be

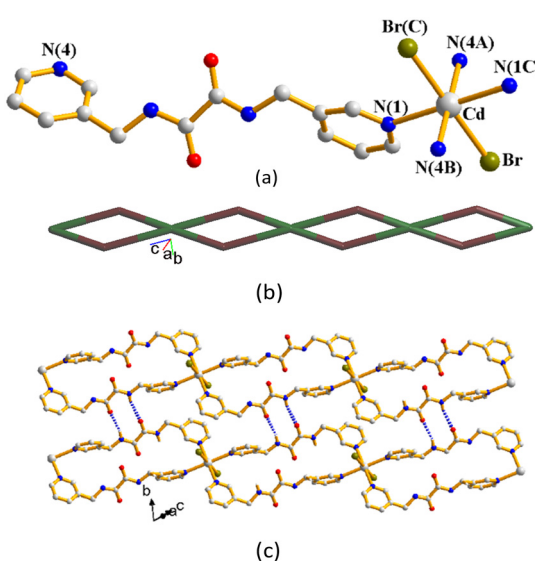


Fig. 7 (a) Coordination environment of $Cd^{(II)}$ in **8**. Symmetry transformations used to generate equivalent atoms: (A) $-x + 2, -y - 1, -z + 1$; (B) $x + 1, y - 1, z + 1$; (C) $-x + 3, -y 2, -z + 2$. (b) A drawing showing the 1D looped chain with the 2,4C4 topology. (c) The adjacent 1D looped chains are interlinked by the $N-H\cdots O$ hydrogen bonds.



regarded as a 2,4-connected 1D net with the $(4^2)(4)_2$ -2,4C4 topology. Noticeably, the adjacent 1D looped chains are interlinked through extensive N-H \cdots O [H \cdots O = 2.208(3) and 2.377(3) Å; \angle N-H \cdots O = 143.1(2) and 130.9(2)°] hydrogen bonds (Fig. 7(c)).

Structure of 2D-[CdBr₂(L¹)₂]_n, 9

The single-crystal X-ray diffraction analysis shows that **9** crystallizes in the monoclinic space group $P2_1/c$. The asymmetric unit consists of one Cd(II) cation and two L¹ ligands. Fig. 8(a) shows the coordination environment of the Cd(II) metal center, which is six-coordinated by its two original bromine atoms [Cd-Br = 2.7090(3) Å] and four nitrogen atoms from four different ligands [Cd-N = 2.4045(19) and 2.4685(19) Å]. If the Cd(II) ions are considered as four-connected nodes and the L¹ ligands as linkers, the structure of **9** can be simplified as a 4-connected 2D net with the (4⁴·6²)-sql topology as illustrated in Fig. 8(b). The Cd(II) metal atoms are bridged by L¹ ligands with 2D layers, which are supported by the N-H \cdots O [H \cdots O = 2.056(3) Å; \angle N-H \cdots O = 146.6(1)°] hydrogen bonds (Fig. S1†).

Structure of [Cd₂Br₂(ox)(L¹)₂]_n, 10

The single-crystal X-ray diffraction analysis shows that **10** crystallizes in the monoclinic space group $P2_1/c$. The asymmetric unit consists of one Cd(II) cation, two oxalate ligands, one L¹ ligand, and one bromine atom. Fig. 9(a) shows the coordination environment of the Cd(II) metal center, which is six-coordinated by two bromine atoms [Cd-Br = 2.6681(4) and 2.9233(4) Å], two oxygen atoms from two decomposed L¹ ligands [Cd-O = 2.265(2) and 2.301(2) Å] and two nitrogen atoms from two different L ligands [Cd-N = 2.279(2) and 2.404(3) Å]. The Cd(II) metal atoms are bridged together by two decomposed L, bonded to another Cd(II) by one L, and bonded to another Cd(II) via two bromine atoms.

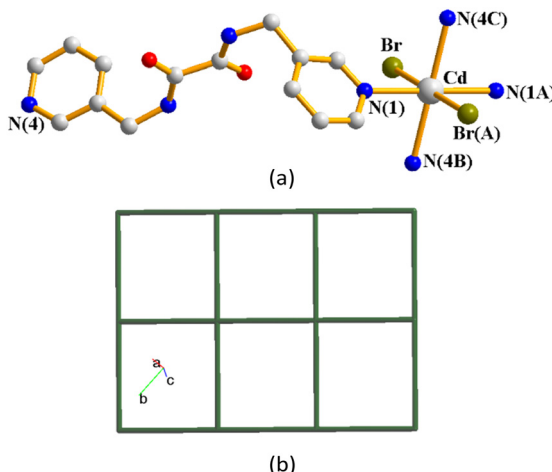


Fig. 8 (a) Coordination environment of Cd(II) in **9**. Symmetry transformations used to generate equivalent atoms: (A) $-x + 1, -y + 2, -z + 2$; (B) $x - 1, -y + 3/2, z + 1/2$; (C) $-x + 2, y + 1/2, -z + 3/2$. (b) A drawing showing the structure of **9** with the sql topology.

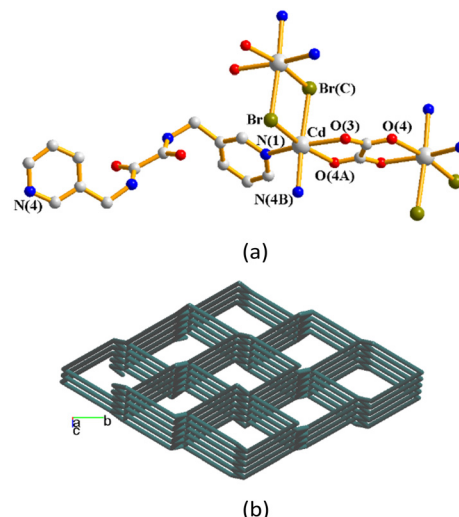


Fig. 9 (a) Coordination environment of Cd(II) in **10**. Symmetry transformations used to generate equivalent atoms: (A) $-x, -y, -z + 1$; (B) $x - 1, -y + 1/2, z + 1/2$; (C) $-x + 1, -y, -z + 1$. (b) A drawing showing the 3D topological structure of **10** with the dia topology.

If the Cd(II) ions are considered as four-connected nodes while the other ligands as linkers, the structure of **10** can be simplified as a 4-connected 3D net with the (6⁶)-dia topology as illustrated in Fig. 9(b), determined using ToposPro.³⁴ The 3D framework is supported by the N-H \cdots O [H \cdots O = 2.223(2) Å; \angle N-H \cdots O = 142.3(2)°] hydrogen bonds (Fig. S2†).

Structure of [[Cd(ox)(L¹)·4H₂O]_n, 11

Complex **11** crystallizes in the monoclinic space group $C2/c$. The asymmetric unit consists of a half of a Cd(II) cation, a half of an L¹ ligand, a half of an oxalate anion and two co-crystallized water molecules. Fig. 10(a) shows the coordination environment of the Cd(II) metal center, which is six-coordinated by two nitrogen atoms from two L¹ ligands [Cd-N = 2.3252(19) Å] and four oxygen atoms from two oxalate anions [Cd-O = 2.2959(15) and 2.3185(16) Å]. The Cd(II) ions are linked by the L¹ ligands and oxalate anions to form a 2D layer (Fig. 10(b)) supported by the double helical chains (Fig. 10(c)). If the Cd(II) ions are considered as four-connected nodes and the L¹ ligands and oxalate anions as linkers, the structure of **11** can be simplified as a 4-connected 2D net with the (4⁴·6²)-sql topology as illustrated in Fig. 10(d). The 2D layers are supported by the O-H \cdots O hydrogen bonds from the water hydrogen atoms to the oxalate oxygen atoms [H \cdots O = 2.035(2) Å; \angle O-H \cdots O = 155.9(1)°], the amide oxygen atoms [H \cdots O = 1.904(2) Å; \angle O-H \cdots O = 168.4(1)°] and the water oxygen atoms [H \cdots O = 1.983(2) and 2.055(2) Å; \angle O-H \cdots O = 163.9(2) and 144.9(2)°] (Fig. S3†).

Ligand conformations and bonding modes

L³ can be arranged in A and G conformations when the C-C-C torsion angles (θ) are $180 \geq \theta > 90^\circ$ and $0 \leq \theta \leq 90^\circ$, respectively, and based on the relative orientation of the

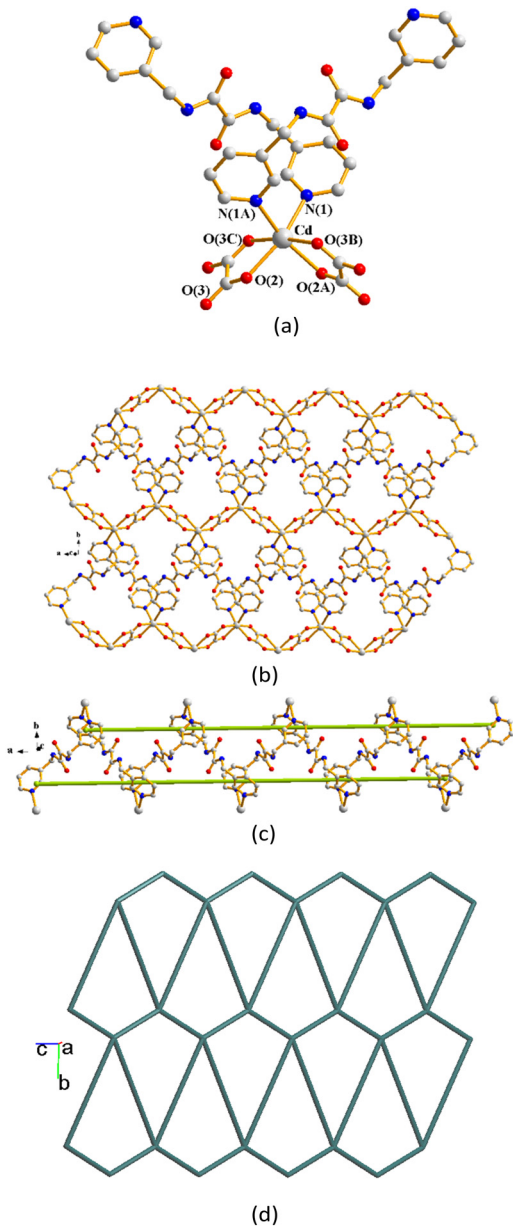


Fig. 10 (a) Coordination environment of Cd(II) in **11**. Symmetry transformations used to generate equivalent atoms: (A) $-x + 1, y, -z + 3/2$; (B) $x, -y + 1, z + 1/2$; (C) $-x + 1, -y + 1, -z + 1$. (b) A drawing showing the 2D layer structure. (c) A drawing showing the double helical structure. (d) A drawing showing the 2D net with the sq1 topology.

C=O groups, each conformation can adopt *cis* or *trans* arrangement.³⁵ Due to the difference in the orientations of the pyridyl nitrogen atom positions, three more orientations, *anti-anti*, *syn-anti* and *syn-syn*, are possible for the ligands L¹–L³. Accordingly, the ligand conformations of **1–11** are assigned and listed in Table 1.

Structural comparisons

Structural comparisons of complexes **1–11** indicate that the subtle structural difference in the 1D zigzag chains of **4** and

Table 1 Ligand conformations of **1–11**

1		2	
	<i>trans syn-anti</i>		<i>trans syn-syn</i>
3		4	
	<i>trans syn-syn</i>		<i>trans syn-syn</i>
5		6	
	<i>trans anti-anti</i>		<i>AAA trans syn-syn</i>
7		8	
	<i>AAG cis anti-syn</i>		<i>trans syn-anti</i>
9		10	
	<i>trans syn-syn</i>		<i>trans syn-syn</i>
11			
	<i>trans syn-syn</i>		

5 is due to the different donor atom positions of the bpba ligands, whereas the difference between **5** and **6** can be ascribed to the ligand flexibility. Moreover, the structural difference between **6** and **7** is attributable to the metal identity. Table 2 lists the structures of the reported d¹⁰-metal halide complexes containing bpba ligands. It is interesting to note that regardless of the flexibility and the shapes of the bpba ligands, only 0D and 1D structures can be obtained for the Zn(II) and Hg(II) halide complexes, whereas higher dimensionality can be achieved for the Cd(II) halide ones. The combined effect of the sizes of the metal centers and halide anions may thus play an important role in determining the dimensionality of the d¹⁰-metal halide complexes containing bpba ligands. Complex **10** represents a rare example that a Cd(II) halide CP is supported by three different ligands.

Powder X-ray analysis

In order to check the phase purity of the products, powder X-ray diffraction (PXRD) experiments have been carried out for complexes **1–11**. As shown in Fig. S4–S14,† the peak positions of the experimental and simulated PXRD patterns are in agreement with each other, except complex **1**, which has been transformed into complex **2** upon solvent removal, *vide infra*.

Supramolecular isomerism and structural transformation

Supramolecular isomers are network structures comprising identical chemical compositions but differ from one



Table 2 d^{10} -Metal halide complexes containing bpba ligands

Complex	Structure	References
$\{[ZnCl_2(L^4)] \cdot H_2O\}_n$	1D double-stranded helical chain	36
$\{[ZnBr_2(L^4)] \cdot H_2O\}_n$	1D double-stranded helical chain	36
$\{[ZnI_2(L^4)] \cdot H_2O\}_n$	1D sinusoidal chain	36
$[Zn_2Cl_4(L^4)_2] \cdot 2DMF$	Dinuclear metallocycle	36
$[Zn_2Br_4(L^4)_2] \cdot 2DMF$	Dinuclear metallocycle	36
$[Zn_2I_4(L^4)_2] \cdot 4DMF \cdot C_4H_{10}O$	Dinuclear metallocycle	36
$\{[HgBr_2(L^5)] \cdot H_2O\}_n$	1D zigzag chain	37
$\{[ZnCl_2(L^6)] \cdot 2DMF \cdot C_4H_{10}O\}_n$	1D zigzag chain	38
$\{[ZnBr_2(L^6)] \cdot 2DMF\}_n$	1D zigzag chain	38
$\{[ZnI_2(L^6)] \cdot 2DMF\}_n$	1D concavo-convex chain	38
$[HgCl_2(L^6)]_n$	1D zigzag chain	38
$\{[HgBr_2(L^6)] \cdot 2DMF\}_n$	1D zigzag chain	38
$Hg_2I_4(L^6)_2$	Dinuclear metallocycle	38
$[HgBr_2(GAG-L^7)]_n$	1D double helical chain	28
$[HgBr_2(AAA-L^7)]_n$	1D helical chain	28
$[HgI_2(GAG-L^7)]_n$	1D sinusoidal chain	28
$[HgI_2(AAA-L^7)]_n$	1D helical chain	28
$[HgCl_2(L^8)]_n$	1D zigzag chain	23
$[HgBr_2(L^8)]_n$	1D zigzag chain	23
$[HgI_2(L^8)]_n$	1D zigzag chain	23
$[HgI_2(L^8) \cdot MeOH]_n$	1D helical chain	23
$[HgI_2(L^8) \cdot MeCN]_n$	1D helical chain	23
$[HgCl_2(L^9)]_n$	1D helical chain	23
$[HgBr_2(L^9)]_n$	1D helical chain	24
$[HgI_2(L^9)]_n$	1D helical chain	24
$\{[HgBr_2(L^9)] \cdot MeCN\}_n$	1D double helical chain	24
$\{[HgI_2(L^9)] \cdot MeCN\}_n$	1D double helical chain	24
$\{[HgCl_2(L^{10})] \cdot CH_3OH\}_n$	1D sinusoidal chain	39
$[HgCl_2(L^{10})]_n$	1D helical chain	39
$[HgBr_2(L^{10})]_n$	1D helical chain	39
$[HgI_2(L^{10})]_n$	1D helical chain	39
$[HgCl_2(L^{11})]_n$	1D helical chain	39
$[HgBr_2(L^{11})]_n$	1D helical chain	40
$[HgI_2(L^{11})]_n$	1D helical chain	40
$[HgBr_2(L^{12})]_n$	1D zigzag chains	30
$[HgI_2(L^{12})]$	Mononuclear complex	30
$[Hg_2Cl_4(L^{13})_2]$	Dinuclear metallocycle	30
$[Hg_2Br_4(L^{13})_2]$	Dinuclear metallocycle	30
$[Hg_2I_4(L^{13})_2]$	Dinuclear metallocycle	30
$\{[HgCl_2(L^{14})] \cdot H_2O\}_n$	1D zigzag chain	30
$\{[HgBr_2(L^{14})] \cdot H_2O\}_n$	1D zigzag chain	30
$\{[HgI_2(L^{14})] \cdot H_2O\}_n$	1D zigzag chain	30
$\{[ZnI_2(L^1)] \cdot 2DMF\}_n, 1$	1D concavo-convex chain	This work
$[ZnI_2(L^1)]_n, 2$	1D zigzag chain	This work
$[CdI_2(L^1)]_n, 3$	1D zigzag chain	This work
$[HgI_2(L^1)]_n, 4$	1D zigzag chain	This work
$[HgI_2(L^2)]_n, 5$	1D zigzag chain	This work
$[Hg_2I_4(L^3)]_n, 6$	Dinuclear complex	This work
$[CdI_2(L^3)]_n, 7$	1D zigzag chain	This work
1D- $[CdBr_2(L^1)_2]_n, 8$	1D looped-chain	This work
2D- $[CdBr_2(L^1)_2]_n, 9$	2D layer with $(4^4 \cdot 6^2)$ -sqI topology	This work
$[Cd_2Br_2(ox)(L^1)_2]_n, 10$	3D framework with (6^6) -dia topology	This work

$L^4 = N,N'$ -di(4-pyridyl)adipoamide; $L^5 = N,N'$ -bis(2-pyrimidinyl)-1,4-benzeneddicarboxamide; $L^6 = N,N'$ -di(3-pyridyl)oxamide; $L^7 = N,N'$ -di(3-pyridyl)adipoamide; $L^8 = 2,2'$ -(1,2-phenylene)-bis(*N*-pyridin-3-yl)acetamide; $L^9 = 2,2'$ -(1,3-phenylene)-bis(*N*-pyridin-3-yl)acetamide; $L^{10} = 2,2'$ -(1,4-phenylene)-bis(*N*-pyridin-3-yl)acetamide; $L^{11} = N,N'$ -di(pyridin-3-yl)naphthalene-1,4-dicarboxamide; $L^{12} = N,N'$ -bis(3-pyridyl)bicyclo(2,2,2,0)oct-7-ene-2,3,5,6-tetracarboxylic diamide; $L^{13} = N,N'$ -bis(4-pyridylmethyl)bicyclo(2,2,2,0)oct-7-ene-2,3,5,6-tetracarboxylic diamide; $L^{14} = 4,4'$ -oxybis(*N*-pyridine-3-yl)benzamide).

another in their structures.⁴¹ Complexes **1** and **2** as well as **8** and **9** thus form two pairs of supramolecular isomers. Importantly, supramolecular isomers prepared under various experimental conditions may be considered

as potential candidates for structural transformation. Consequently, the investigation of both supramolecular isomerism and structural transformation may prove crucial for advancing the crystal engineering of CPs.



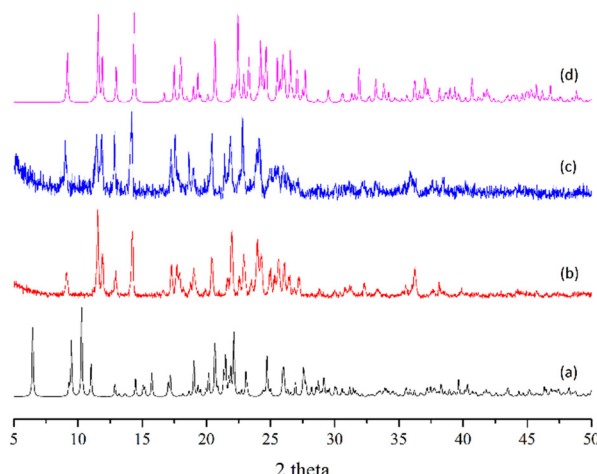


Fig. 11 (a) Simulated PXRD pattern of **1**, (b) PXRD pattern of the as-synthesized **1** exposed to air for five minutes, (c) PXRD pattern of the sample of (b) immersed in DMF and (d) simulated PXRD pattern of **2**.

Structural transformation in complexes **1** and **2**

Complexes **1** and **2** provide an opportunity to investigate the structural transformation due to the removal of DMF molecules in the zinc(II) CPs. The structure of the as-synthesized complex **1** which contains DMF was not stable. When it was exposed to air for 5 minutes, the experimental PXRD pattern (Fig. 11(b)) shows a similar pattern to that of complex **2** (Fig. 11(d)), indicating structural transformation from **1** to **2** upon the removal of the DMF molecules. When the desolvated sample of **1** was immersed in DMF, the PXRD pattern (Fig. 11(c)) reveals no significant change. The irreversible structural transformation from **1** to **2** probably indicates that the self-complementary N-H \cdots O hydrogen bonds in **2** that link the 1D chains may be much stronger than the N-H \cdots O hydrogen bonds in **1** that link the 1D chains and DMF solvents.

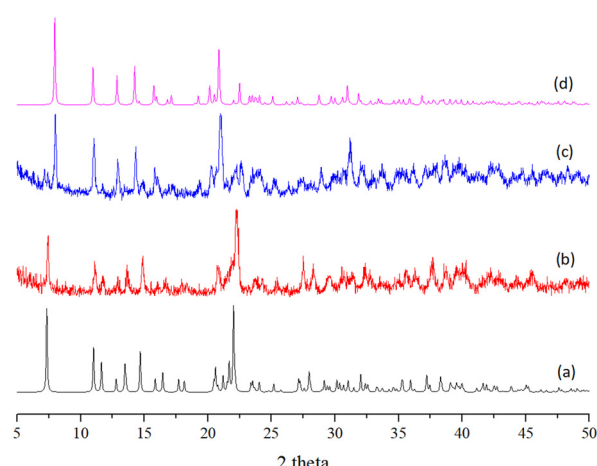


Fig. 12 (a) Simulated PXRD pattern of **8**, (b) PXRD pattern of the as-synthesized **8**, (c) PXRD pattern of the sample of (b) heated in water at 100 °C for 2 days and (d) simulated PXRD pattern of **9**.

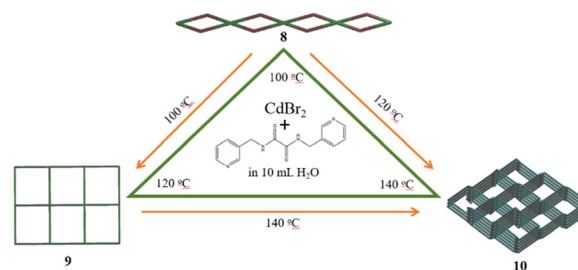


Fig. 13 A drawing showing the formation pathways of complexes **8-10** as well as their structural transformations.

Structural transformation in complexes **8-10**

In order to achieve the structural transformations, complex **8** was hydrothermally heated at 100 and 120 °C, respectively, for 48 hours. The PXRD patterns (Fig. 12 and S15 \dagger) indicate that the structure of **8**, originally a 1D structure, has been changed into a 2D layer precisely alike **9**, and a 3D framework of **10**, respectively. On the other hand, heating **9** hydrothermally at 140 °C leads to the formation of **10**, as demonstrated by the PXRD patterns shown in Fig. S16. \dagger Fig. 13 depicts a drawing showing the formation pathways of complexes **8-10** and their corresponding structural transformations. Noticeably, the independent structural transformations from **8** to **10** and **9** to **10** have led to the decomposition of the L^1 ligands and subsequently the formation of the oxalate anions (ox^-). The ox^- anion can also be observed in the structure of complex **11**, which was prepared at 120 °C by using the starting metal salt $\text{Cd}(\text{CH}_3\text{COO})_2 \cdot 2\text{H}_2\text{O}$, probably indicating that the halide anion is not important in the decomposition of the L^1 ligand.

Conclusions

Ten new CPs and one dinuclear complex supported by the bpba ligands have been successfully obtained, in which complexes **1-10** are d^{10} -metal halides. Their structural types are susceptible to the changes of the ligand isomerism and flexibility as well as the metal identity. Complexes **1-4** represent a unique example demonstrating that the cocrystallized DMF molecules play a more important structure-directing role than the metal identity. Irreversible structural transformation from complex **1** to complex **2** upon DMF removal has been demonstrated, presumably owing to the conformational change of the L^1 ligand. The formation of **8-10** is temperature-dependent, affording a 1D chain, a 2D layer and a 3D framework, respectively. Complexes **10** and **11** were obtained on account of the decomposition of the L^1 ligand, leading to the formation of the ox^- anion. Structural transformations in **8-10** are observed, resulting in the conformational change of L^1 in **8** to **9** and ligand decomposition in **8** to **10** and **9** to **10**. Careful evaluation of the reaction temperature may thus lead to the observation of unique structural alterations. Structural comparisons of the reported bpba-based Zn(II), Cd(II) and Hg(II) halide complexes indicate that only 0D and 1D structures can be obtained for



the Zn(II) and Hg(II) halide complexes, while higher dimensionality can be achieved for the Cd(II) halide ones, irrespective of the increasing size Zn(II) < Cd(II) < Hg(II).

Data availability

The data supporting this article have been included as part of the ESI.† Crystallographic data for complexes 1–11 have been deposited at the CCDC with no. 2445340–2445350.

Author contributions

Investigation, A. R., H.-C. Z., Y.-S. L., Y.-H. Y., Y.-T. K. and Y.-F. L.; data curation, Z.-L. C. and S.-W. W.; review and supervision, J.-D. C. All authors have read and agreed to the published version of the manuscript.

Conflicts of interest

There are no conflicts to declare.

Acknowledgements

We are grateful to the National Science and Technology Council of the Republic of China for support.

References

- W. P. Lustig, S. Mukherjee, N. D. Rudd, A. V. Desai, J. Li and S. K. Ghosh, *Chem. Soc. Rev.*, 2017, **46**, 3242–3285.
- S. R. Batten, S. M. Neville and D. R. Turner, *Coordination Polymers Design, Analysis and Application*, The Royal Society of Chemistry, London, UK, 2009.
- S. Mondal and P. Dastidar, *Cryst. Growth Des.*, 2020, **20**, 7411–7420.
- V. Chandrasekhar, C. Mohapatra, R. Banerjee and A. Mallick, *Inorg. Chem.*, 2013, **52**, 3579–3581.
- J. Yu, Y. Cheng, X. Zhang, L. Zhou, Z. Song, A. Nezamzadeh-Ejhieh and Y. Huang, *J. Environ. Chem. Eng.*, 2025, **13**, 116870.
- P. Yan, Z. Chen, X. Li, F. Liang, Y. Tan, Y. Lin, K. Yang, C. Xiao, J. Wu and D. Ma, *J. Solid State Chem.*, 2024, **330**, 124461.
- F. Liang, D. Ma, L. Qin, Q. Yu, J. Chen, R. Liang, C. Zhong, H. Liao and Z. Peng, *Dalton Trans.*, 2024, **53**, 10070–10074.
- Y. Zhang, H. Tan, J. Zhu, L. Duan, Y. Ding, F. Liang, Y. Li, X. Peng, R. Jiang, J. Yu, J. Fan, Y. Chen, R. Chen and D. Ma, *Molecules*, 2024, **29**, 5903.
- V. Lakshmanan, Y.-T. Lai, X.-K. Yang, M. Govindaraj, C.-H. Lin and J.-D. Chen, *Polymer*, 2021, **13**, 3018.
- W.-T. Lee, T.-T. Liao and J.-D. Chen, *Int. J. Mol. Sci.*, 2022, **23**, 3603.
- V. Lakshmanan, C.-Y. Lee, Y.-W. Tseng, Y.-H. Liu, C.-H. Lin and J.-D. Chen, *CrystEngComm*, 2022, **24**, 6076–6086.
- J. L. Sague, M. Meuwly and K. M. Fromm, *CrystEngComm*, 2008, **10**, 1542–1549.
- J. J. Vittal, *Coord. Chem. Rev.*, 2007, **251**, 1781–1795.
- G. K. Kole and J. J. Vittal, *Chem. Soc. Rev.*, 2013, **42**, 1755–1775.
- G. Chakraborty, I.-H. Park, R. Medishetty and J. J. Vittal, *Chem. Rev.*, 2021, **121**, 3751–3891.
- C.-H. Hsu, W.-C. Huang, X.-K. Yang, C.-T. Yang, P. M. Chhetri and J.-D. Chen, *Cryst. Growth Des.*, 2019, **19**, 1728–1737.
- X.-K. Yang and J.-D. Chen, *CrystEngComm*, 2019, **21**, 7437–7446.
- Y.-F. Liu, J.-H. Hu, W.-T. Lee, X.-K. Yang and J.-D. Chen, *Cryst. Growth Des.*, 2020, **20**, 7211–7218.
- C.-Y. Lee, Y.-H. Ye, S.-W. Wang and J.-D. Chen, *Molecules*, 2024, **29**, 1748.
- C.-Y. Lee, M. Usman, S.-W. Wang, K. B. Thapa, T.-R. Chen and J.-D. Chen, *CrystEngComm*, 2024, **26**, 5099–5107.
- X. Hao, Y.-X. Wang, Y. Yang, Z. Song, X. Dong, S. Wang, Y. Liang, L. Li and P. Cheng, *Cryst. Growth Des.*, 2025, **25**, 2792–2797.
- A. Morsali and M. Y. Masoomi, *Coord. Chem. Rev.*, 2009, **253**, 1882–1905.
- P. M. Chhetri, X.-K. Yang and J.-D. Chen, *Cryst. Growth Des.*, 2017, **17**, 4801–4809.
- P. M. Chhetri, X.-K. Yang and J.-D. Chen, *CrystEngComm*, 2018, **20**, 2126–2134.
- G. Mahmoudi, J. K. Zareba, A. Bauzá, M. Kubicki, A. Bartyzel, A. D. Keramidas, L. Butusov, B. Miroslaw and A. Frontera, *CrystEngComm*, 2018, **20**, 1065–1076.
- L. K. Rana, S. Sharma and G. Hundal, *Cryst. Growth Des.*, 2016, **16**, 92–107.
- G. Mahmoudi, A. Bauzá, A. V. Gurbanov, F. I. Zubkov, W. Maniukiewicz, A. Rodriguez-Díéguez, E. López-Torres and A. Frontera, *CrystEngComm*, 2016, **18**, 9056–9066.
- K. B. Thapa, Y.-F. Hsu, H.-C. Lin and J.-D. Chen, *CrystEngComm*, 2015, **17**, 7574–7582.
- S. M. Mobin, A. K. Srivastava, P. Mathur and G. K. Lahiri, *Dalton Trans.*, 2010, **39**, 8698–8705.
- M. Govindaraj, W.-C. Huang, C.-Y. Lee, V. Lakshmanan, Y.-H. Liu, P. B. So, C.-H. Lin and J.-D. Chen, *Int. J. Mol. Sci.*, 2022, **23**, 7861.
- J.-H. Hu, H.-H. Hsu, Y.-W. Chen, W.-H. Chen, S.-M. Liu and J.-D. Chen, *J. Mol. Struct.*, 2023, **1289**, 135896.
- Bruker AXS, APEX2, V2008.6, SADABS V2008/1, SAINT V7.60A, SHELXTL V6.14, Bruker AXS Inc., Madison, WI, USA, 2008.
- G. M. Sheldrick, *Acta Crystallogr., Sect. A*, 2008, **64**, 112–122.
- V. A. Blatov, A. P. Shevchenko and D. M. Proserpio, *Cryst. Growth Des.*, 2014, **14**, 3576–3586.
- K. B. Thapa and J.-D. Chen, *CrystEngComm*, 2015, **17**, 4611–4626.
- Y.-F. Hsu, W. Hsu, C.-J. Wu, P.-C. Cheng, C.-W. Yeh, W.-J. Chang, J.-D. Chen and J.-C. Wang, *CrystEngComm*, 2010, **12**, 702–710.
- T.-P. Tsai, Y.-T. Huang, U. Ray, Y.-J. Chang, P.-C. Cheng, C.-J. Wu, J.-D. Chen and J.-C. Wang, *Polyhedron*, 2010, **29**, 3081–3088.



38 H.-L. Hua, Y.-F. Hsu, C.-J. Wu, C.-W. Yeh, J.-D. Chen and J.-C. Wang, *Polyhedron*, 2012, **33**, 280–288.

39 P. M. Chhetri, X.-K. Yang, C.-T. Yang and J.-D. Chen, *Polymer*, 2019, **11**, 436.

40 P. M. Chhetri, X.-K. Yang and J.-D. Chen, *J. Mol. Struct.*, 2021, **1239**, 130543.

41 J.-P. Zhang, X.-C. Huang and X.-M. Chen, *Chem. Soc. Rev.*, 2009, **38**, 2385–2396.

